RESEARCH ARTICLE

NANO · MICRO small
www.small-journal.com

Balance Between Oxygen 2p Holes and Oxygen Vacancies for Optimal Water Oxidation

Gao Chen, Yiran Ying, Sixuan She, Yanping Zhu, Zhiwei Hu,* Jiayi Tang, Xubin Ye, Youwen Long, Chang-Yang Kuo, Chien-Te Chen, Dongsheng Geng, Haitao Huang,* and Zongping Shao**

The emergence of the lattice oxygen-mediated mechanism (LOM) has triggered a paradigm shift in oxygen evolution reaction (OER) research from conventional metal-centered catalysis to the reactivity of lattice oxygen sites. In LOM scenario, one viewpoint is that the degree of metal-oxygen covalency controls the OER activity, while the other argument suggests the determining factor is oxygen vacancy. However, metal-oxygen covalency has a competing relationship with oxygen vacancy. Herein, it is demonstrated that the intrinsic OER activity of cobaltite perovskites would be more accurately described by considering two competing factors on the O sites, i.e., oxygen 2p hole (an indicator of metal-oxygen covalency) and oxygen vacancy simultaneously. The increment in oxygen 2p hole favors the LOM route but weakens the hydroxide affinity, whereas moderate oxygen vacancy mitigates the undesirable effects of high oxygen 2p hole. Specifically, the $Sr_{0.9}Y_{0.1}CoO_{3-\delta}$ catalyst among $Sr_{1-x}Y_xCoO_3$ system has an ideal balance between oxygen 2p hole and oxygen vacancy, catalyzes OER via LOM, showing the optimal intrinsic activity. The proposed dual-parameter descriptor offers a coherent explanation for the OER activity of cobaltite perovskites, and more importantly, it would shed light on future design of efficient OER electrocatalysts under the classic Sabatier principle.

1. Introduction

Electrocatalytic oxygen evolution reaction (OER) driven by externally applied potentials is the efficiency-limiting factor for many vital electrochemical applications, for example, hydrogen (H_2) production via water splitting.[1–3] There are three typical electrolyzers for water splitting, proton exchange membrane (PEM), alkaline liquid electrolyte (ALE), and anion exchange membrane (AEM) electrolyzers. The commercial PEM electrolyzer enables fast response to intermittent renewable energy and produces high-purity H_2 using expensive IrO_2 as OER catalysts. The commercial ALE electrolyzer can use non-precious metal catalysts, but the start-up response to intermittent renewable energy is slow, and the produced hydrogen is impure. Combining the advantages of ALE and PEM systems, the AEM electrolyzer can produce high-purity hydrogen with a quick response to intermittent renewable energy under alkaline conditions, allowing the use of non-noble metal catalysts. However, the development of anion exchange membrane electrolyzer is in the early stage, and there is still a large room for improvement in device efficiency when non-noble metal catalysts are employed.[4]

Identifying the physicochemical properties that affect OER activity and accordingly tailoring catalysts to optimize their OER performance are crucial to advancing anion-exchange membrane

G. Chen, D. Geng
Jiangsu Key Laboratory of New Energy Devices and Interface Science
School of Chemistry and Materials Science
Nanjing University of Information Science and Technology
Nanjing 210044, China
E-mail: gaochen@nuist.edu.cn

Y. Ying, S. She, Y. Zhu, H. Huang
Department of Applied Physics and Research Institute for Smart Energy
The Hong Kong Polytechnic University
Hong Kong 999077, China
E-mail: aphhuang@polyu.edu.hk

Z. Hu
Max-Planck-Institute for Chemical Physics of Solids
Nöthnitzer Street 40, 01187 Dresden, Germany
E-mail: zhiwei.Hu@cpfs.mpg.de

The ORCID identification number(s) for the author(s) of this article can be found under https://doi.org/10.1002/smll.202512440

DOI: 10.1002/smll.202512440

J. Tang, Z. Shao
WA School of Mines: Minerals
Energy and Chemical Engineering
Curtin University
Perth, WA 6102, Australia
E-mail: zongping.shao@curtin.edu.au

X. Ye, Y. Long
Beijing National Laboratory for Condensed Matter Physics
Institute of Physics
Chinese Academy of Sciences
Beijing 100190, China

C.-Y. Kuo, C.-T. Chen
National Synchrotron Radiation Research Center
101 Hsin-Ann Road, Hsinchu 30076, Taiwan

C.-Y. Kuo
Department of Electrophysics
National Yang Ming Chiao Tung University
Hsinchu 300, Taiwan

electrolyzer technology.[5,6] Cobaltite perovskites ($ACoO_{3-\delta}$, A = alkaline or rare earth elements, and δ represents the value of oxygen vacancy) with tunable structure and decent OER performance have played a landmark role in correlating physicochemical property and OER activity.[7–11] The physicochemical property can be regarded as an activity "descriptor" for designing new efficient catalysts. For instance, Shao-Horn and coworkers have found that the e_g filling of Co close to unity has moderate binding strength to oxygenated intermediates, which could help predict the highly active $Ba_{0.5}Sr_{0.5}Co_{0.8}Fe_{0.2}O_{3-\delta}$ catalyst.[7] Further, the Keith and Shao-Horn groups have demonstrated that the lattice O in $La_{(1-x)}Sr_xCoO_{3-\delta}$ with strong Co-O covalency is more active than Co site for OER, and $SrCoO_{3-\delta}$ with considerable Co-O covalency provides the best OER activity among the $La_{(1-x)}Sr_xCoO_{3-\delta}$ electrodes.[8,10] With the discovery of lattice oxygen involvement, the lattice oxygen-participation mechanism (LOM) is established alongside the conventional adsorbate evolution mechanism (AEM). As LOM would break the scaling relationship in conventional AEM and lead to better OER activity, the oxygen site has become the center of attention in OER study. Meanwhile, Keith and colleagues have proposed oxygen vacancy as a decisive factor for OER activity via LOM.[10] Recently, Emiliana and coworkers have unveiled the quantitative relation between the content of oxygen vacancy in $PrBaCo_2O_{5+\delta}$ and the corresponding OER activity, in which more oxygen vacancy corresponds to higher OER activity.[12]

Inspired by the above findings, many studies have focused on developing catalysts with rich oxygen vacancies or strong metal-oxygen covalency to improve OER activity.[13–19] Nevertheless, when these two factors are considered simultaneously, the situation becomes confused. Typically, Co-O covalency refers to the orbital overlap of Co 3*d* and O 2*p*. In the condition of strong covalency, an electron on O site would transfer to Co, resulting in an electron-defective (hole-rich) state on O.[20] The content of the oxygen 2*p* hole is positively correlated to the degree of Co-O covalency. Oxygen 2*p* hole refers to the loss of electrons from the outer-shell orbital of oxygen atoms, whereas oxygen vacancy refers to the loss of oxygen atoms from the perovskite lattice. Increasing Co valence state enlarges the content of the oxygen 2*p* hole, which would lift the risk of structural instability, resulting in the creation of an oxygen vacancy. Consequently, the valence state of Co should decrease to maintain charge balance, thereby in turn reducing the oxygen 2*p* hole. In a word, in perovskite, oxygen vacancy and oxygen 2*p* hole are competing factors, and the content of oxygen vacancy increases at the expense of oxygen 2*p* holes and Co-O covalency. In this regard, notions that both enhance Co-O covalency and oxygen vacancy to improve OER activity seem conflicting. Considering two extreme cases: 1) when the degree of Co-O covalency reaches the maximum value, it will cause an extremely weak hydroxide affinity;[21] 2) excessive oxygen vacancies will enlarge the bandgap and lower the O 2*p* band center,[22] both of which are inconsistent with the prediction for optimum catalysts under the Sabatier principle.

Herein, we use a series of cobaltite perovskites ($Sr_{(1-x)}Y_xCoO_{3-\delta}$ (x = 0, 0.1, 0.2, 0.3, 0.5, and 1)) and CoO as a model material system to establish the relationship between oxygen vacancy/2*p* hole and OER activity/mechanism. The $Sr_{(1-x)}Y_xCoO_{3-\delta}$ system was employed as a model catalyst platform due to its large tunable region of both oxygen vacancy and oxygen 2*p* hole. Among them, $Sr_{(1-x)}Y_xCoO_{3-\delta}$ (x = 0, 0.5, and 1, denoted as SC-*HP*, $S_{0.5}Y_{0.5}$C-*HP*, and YC-*HP*, respectively) with minimal oxygen vacancies were prepared under high pressure; $Sr_{(1-x)}Y_xCoO_{3-\delta}$ (x = 0, 0.1, 0.2, and 0.3, denoted as SC, $S_{0.1}Y_{0.9}$C, $S_{0.2}Y_{0.8}$C, and $S_{0.3}Y_{0.7}$C, respectively)) with large content of oxygen vacancies were synthesized under atmospheric pressure. By using surface-sensitive soft X-ray absorption spectroscopy (XAS) measurements and density functional theory (DFT) calculations, we conclude that balancing the degree of oxygen 2*p* hole and oxygen vacancy in cobaltite perovskites is the key to achieving optimal OER activity. We further assemble an anion exchange membrane electrolyzer using the optimal $S_{0.9}Y_{0.1}$C as anode and Pt as cathode, which outperforms the state-of-the-art IrO_2/Pt catalyst pair. Our findings unify the factors governing anionic redox in electrocatalysis and provide a criterion that complies with the golden Sabatier principle for the rational design of OER catalysts in the LOM pathway.

2. Results and Discussion

X-ray diffraction (XRD) was conducted to reveal the structure of the as-prepared samples. The XRD pattern (**Figure 1a**) reveals that the SC-*HP* sample synthesized under high pressure adopts a cubic structure with a space group of Pm-3*m*, which differs from the common brownmillerite structure (SC) synthesized under atmospheric pressure.[23] The XRD patterns of $S_{0.5}Y_{0.5}$C-*HP* and YC-*HP* could be indexed to cubic and orthorhombic structures, respectively, as illustrated by the previous study.[24] The SYC (x = 0.1, 0.2, and 0.3) samples have a tetragonal structure with a space group of I4/*mmm*, which is consistent with the earlier report.[25] As indicated by the asterisk, the as-synthesized $Sr_{0.7}Y_{0.3}CoO_{3-\delta}$ ($S_{0.7}Y_{0.3}$C) sample contains a small amount of Y_2O_3 impurity, most likely due to the evaporation of cobalt element at high temperatures.[25] CoO has a cubic phase.

Soft XAS was used to reveal the surface electronic structure of the catalysts. Figure 1b displays the Co *L*-edge XAS spectra and their average valence state of all synthesized cobalt oxides. The curve fitting of Co *L*-edge XAS spectra (as illustrated in Figure S1–S6, Supporting Information) was performed by superposing reference spectra including $SrCoO_3$ for intermediate-spin (IS) Co^{4+}, Sr_2CoO_3Cl for high-spin (HS) Co^{3+}, $EuCoO_3$ for low-spin (LS) Co^{3+}, and CoO for HS Co^{2+}. The fitting result indicates an average covalence state of +3.35, +3.3, +3.25, and +3.21 for SC, $S_{0.1}Y_{0.9}$C, $S_{0.2}Y_{0.8}$C, and $S_{0.3}Y_{0.7}$C, respectively. The valence states derived from XAS spectra are lower than their nominal values (6 – the average valence state of A), signifying the presence of oxygen vacancies in the SC and SYC samples generated under atmospheric pressure. As a sharp contrast, the samples prepared under high pressure show valence states that are almost close to their nominal values (Figures S5 and S6, Supporting Information). The Co-*L* XAS spectra of CoO and SC-*HP* are consistent with previous reports that Co^{2+} and Co^{4+} have a HS and IS state, respectively.[26,27]

We further analyzed the corresponding O *K*-edge spectra, which convey information about the oxygen 2*p* hole (also the degree of covalency of Co 3*d* and O 2*p* states).[28] As revealed from the O *K*-edge spectra of the four references including CoO (HS-Co^{2+}), $LaCoO_3$-20K (LS-Co^{3+}), $LaCoO_3$-650K (HS-Co^{3+}) and $SrCoO_3$ (IS-Co^{4+}) in Figure S7 (Supporting Information), with the increase of Co valence, the pre-edge peak of the O *K*-edge

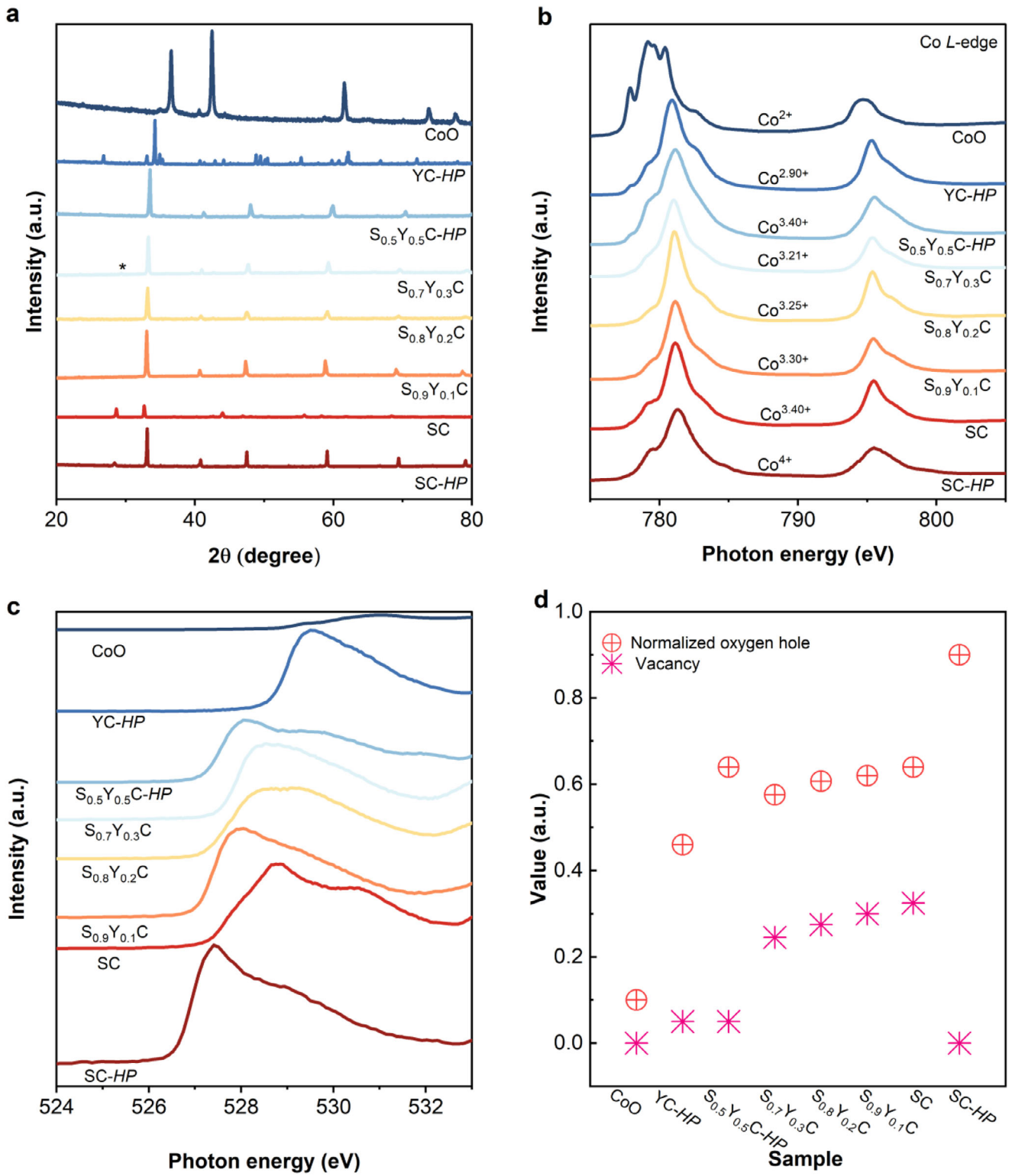

Figure 1. a) XRD patterns, b) Co $L_{2,3}$-edge spectra, and c) pre-edge peaks of O *K*-edge spectra of the as-synthesized samples. d) The content of the normalized O 2*p* hole and oxygen vacancy of the as-synthesized samples. The asterisk in (a) indicates a small amount of Y_2O_3 impurity.

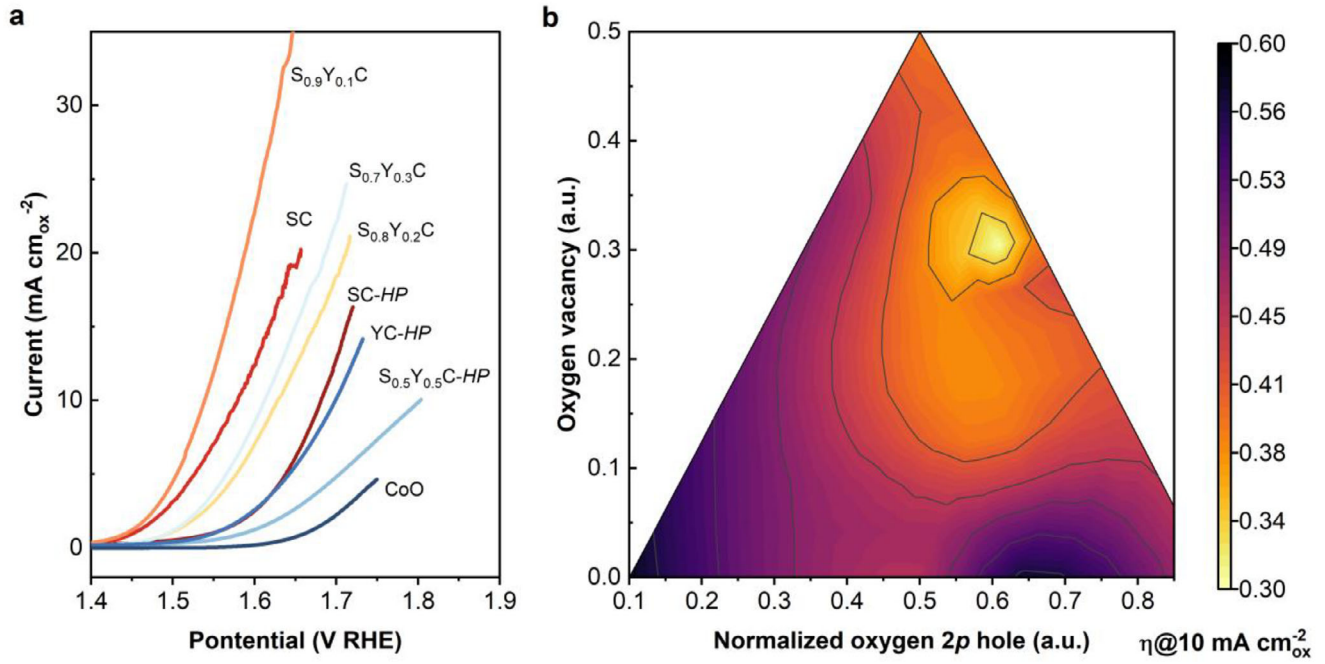

Figure 2. a) The intrinsic OER activity of the cobalt oxides. b) A summary of two competing parameters (oxygen vacancy and normalized O 2*p* hole) and η@10 mA cm-2 ox of studied and previously reported cobaltite perovskites ($LaCoO_3$,[10] $SrCoO_{3-\delta}$ ($SrCoO_{2.5}$),[10] $SrSi_{0.05}Co_{0.95}O_{3-\delta}$, $Pr_{0.5}Ba_{0.5}CoO_{3-\delta}$,[32] $LaSr_{1.9}Co_{1.5}Fe_{1.5}O_{9-3\delta}$,[33] $SrNb_{0.1}Co_{0.7}Fe_{0.2}O_{3-\delta}$,[34] and $SrCo_{0.4}Fe_{0.2}W_{0.4}O_{3-\delta}$[35]).

shifts to lower energy and the peak intensity increases, which indicates the increasing content of oxygen 2*p* hole. Although having the same Co oxidation state, the content of oxygen 2*p* hole of Co^{3+} (HS)-O is larger than that in the Co^{3+} (LS)-O (Figure S7, Supporting Information). This is attributed to more electron filling in the higher-energy e_g orbital in the electron configuration of HS-Co^{3+}. Figure 1c shows the pre-edge peak of the O *K*-edge of the tested cobaltite oxides. The content of the O 2*p* hole in each cobaltite oxide can be estimated by integrating the pre-edge peak of the O *K*-edge. The integrated area can be used as an indicator of the O 2*p* hole.

Furthermore, we quantified the oxygen vacancy and O 2*p* hole of these cobalt oxides based on the above XAS results. The value of oxygen vacancy, i.e., δ, can be calculated via $\delta = 0.5 \times (6\text{-A-B})$, where A and B represent the average valence state of A-site and B-site cations, respectively. The average valence state of A-site cations is calculated by $[2 \times (1\text{-x}) + 3\text{x}]$, where x represents the ratio of Y^{3+} in the A site. The average valence state of B-site cations is obtained from the XAS results as shown in Figure 1b. To make sure the content of the O 2*p* hole is equivalent to the valence state, the integrated area obtained in Figure 1c was converted into a normalized value as the following procedures:

1) The Co 3*d* electrons can be described by the wave function of $\Phi = \alpha|3d^n > + \beta|3d^{n+1} > L$, where $\underline{L}$ represents the oxygen ligand hole. According to previous reports,[29–31] the values of β for Co^{2+}, Co^{3+}, and Co^{4+} are approximately equal to 0.1, 0.5, and 0.9, respectively.
2) Divide the β value by the corresponding integral area to get a coefficient. The average coefficient derived from the above three sets of data is 0.15.
3) By timing the coefficient 0.15, the integral area could be converted into a normalized O 2p hole value, which is an equivalent value to the valence state.

The content of oxygen vacancy and the normalized O 2*p* hole are shown in Figure 1d. Except for CoO, samples synthesized under atmospheric pressure contain higher oxygen vacancies, which increase as the Y content decreases, whereas those synthesized under high pressure exhibit marginal oxygen vacancies. No obvious oxygen vacancy was observed in CoO owing to the large oxygen vacancy formation enthalpy in cobalt oxide with a low valence state.[8] As for oxygen 2*p* hole, samples synthesized under high pressure exhibit oxygen 2*p* holes that are nearly equivalent to their nominal levels. In contrast, those synthesized under atmospheric pressure display oxygen 2*p* holes that are below the nominal values, with their content showing an upward trend as the Y content diminishes. In a perovskite where the A-site valence remains constant, oxygen vacancy and oxygen 2*p* hole compete with each other. However, in the four samples synthesized under atmospheric pressure, the decrease in the average valence of the A-site leads to an increase in cobalt valence. On one hand, this enhances the covalency of Co—O bonds, and on the other hand, it reduces the enthalpy of oxygen vacancy formation. Consequently, both the content of oxygen vacancy and oxygen 2*p* hole increase.

The OER activity of the as-prepared catalysts was evaluated in 0.1 M KOH adopting a three-electrode configuration. **Figure 2a** exhibits the intrinsic activity (normalized to the BET surface area, Table S1, Supporting Information) of the studied electrodes. It is observed that catalysts with negligible oxygen vacancy (SC-*HP*, YC-*HP*, $S_{0.5}Y_{0.5}C$-*HP*, CoO) show worse OER activity than catalysts with have a larger content of oxygen vacancy (SC, $S_{0.9}Y_{0.1}C$,

$S_{0.8}Y_{0.2}C$, $S_{0.7}Y_{0.3}C$). This observation unequivocally supports the critical role of oxygen vacancy in enhancing OER activity. However, despite SC having a higher oxygen vacancy content than $S_{0.9}Y_{0.1}C$, its intrinsic OER activity is weaker, indicating that OER activity is not solely determined by the oxygen vacancy content. A similar conclusion can be drawn from the O 2*p* hole perspective. $S_{0.9}Y_{0.1}C$, which shows the highest OER activity, does not have the highest O 2*p* hole content. The variation trend of intrinsic OER activity does not follow the trends of changing the oxygen 2*p* hole or oxygen vacancy.

Figure 2b depicts a contour plot to uncover the underlying connections between oxygen vacancy/oxygen 2*p* hole and intrinsic OER activity of the examined cobalt oxides and a few cobalt-based perovskites reported by different groups. The overpotential that achieves a current density of 10 mA cm−2 ox (η@10 mA cm−2 ox) was used as the indicator of the intrinsic OER activity. From the contour plot, it is evident that the sample with the highest OER activity is located within a specific region, characterized by the conditions 0.60 < O 2*p* hole < 0.64 and 0.28 < oxygen vacancy < 0.32. Specifically, $S_{0.9}Y_{0.1}C$ catalyst shows the highest intrinsic OER activity among the studied cobalt oxides and competitive turnover frequency (TOF) compared with other state-of-the-art OER catalysts (Figure S8, Supporting Information). Our findings reveal that the cobalt oxides exhibiting optimal OER activity have moderate oxygen vacancy and O 2*p* hole contents rather than their limit levels. It should be noted that the arrangement of oxygen vacancies also affects the OER activity.[12] It has been demonstrated that the ordered arrangement of oxygen vacancies affects oxygen ion diffusion, thereby leading to lower OER activity. SC adopts a brownmillerite structure whose oxygen vacancies are arranged in a highly ordered fashion, providing a straightforward structural reason for its slightly inferior performance than $S_{0.9}Y_{0.1}C$.

DFT calculations were performed to illuminate the interplay between oxygen vacancy and O 2*p* hole, offering valuable insights into their combined impact on OER performance. We investigated three different pathways, i.e., adsorbate evolution mechanism (AEM), lattice oxygen-mediated mechanism at metal site (LOM-M), and LOM at oxygen site (LOM-O). Since CoO and SC-*HP* with the smallest and highest Co-O covalency prefer the AEM and LOM routes, respectively, no DFT calculations are performed for CoO under LOM routes and SC-*HP* under the AEM route. During the AEM process, only the surface Co centers serve as catalytically active sites on which the OH^- undergo four concerted proton-electron transfer steps to yield O_2. Figure S9 (Supporting Information) presents the calculated Gibbs free energy diagrams for the CoO and $S_{0.9}Y_{0.1}C$ catalyst via AEM, respectively. It is found that the potential-limiting step (PLS) is the O-O coupling for the CoO catalyst with a reaction Gibbs free energy change (ΔG) of up to 2.43 eV, whereas the hydroxide adsorption step remains the PLS for the $S_{0.9}Y_{0.1}C$ (ΔG = 0.66 eV). As a sharp contrast, the ΔG of hydroxide adsorption on CoO catalyst is −2.29 eV. This result is in good agreement with the previous investigation that metals with high valence and less out shell electrons have weak hydroxide affinity.[11,21] Meanwhile, the LOM involves a lattice-oxygen oxidation and nonconcerted proton-electron transfer. **Figure 3**a,b display the proposed OER pathway on the $S_{0.9}Y_{0.1}C$/ SC-*HP* catalyst with LOM at Co and O site, respectively, and the corresponding free energies of each step were also calculated. Figure 3c,d reveal that $S_{0.9}Y_{0.1}C$ and SC-*HP* prefer the LOM-O and LOM-Co route. As can be seen from Figure 3c (step 3) and Figure 3d (step 4), both the PLS for $S_{0.9}Y_{0.1}C$ in LOM-O and SC-*HP* in LOM-Co are the oxygen vacancy refilling. Since $S_{0.9}Y_{0.1}C$ possesses a lower valence state (and a lower content of normalized oxygen 2*p* hole) than SC-*HP*, its hydroxide affinity and PLS value are superior to those of SC-*HP*. Furthermore, ΔG of oxygen vacancy filling via LOM is smaller than that of hydroxide adsorption via AEM on the $S_{0.9}Y_{0.1}C$ catalyst (Figure 3 vs Figure S9, Supporting Information), confirming that the presence of an oxygen vacancy decreases the Gibbs free energy of PLS. The results from the operando O^{18} isotope labeling experiment detected the presence of $^{34}O_2$ but not $^{36}O_2$ (**Figure 4**), indicating the existence of the single-vacancy lattice oxygen mechanism, which is consistent with the models in DFT calculations. Furthermore, $S_{0.9}Y_{0.1}C$ produced more $^{34}O_2$ than SC-HP, demonstrating that the former has superior OER activity.

Based on the above findings, it is evident that the O 2*p* hole dictates the OER mechanism and the hydroxide affinity. As the O 2*p* hole content increases from low to high, the OER mechanism transitions from the AEM to the LOM. Concurrently, the PLS of OER shifts from O-O coupling to OH^- adsorption via AEM (or oxygen vacancy filling via LOM). The presence of oxygen vacancy can reduce the O 2*p* hole content, thereby enhancing the hydroxide affinity and lowering the PLS of OER. This comprehensive understanding highlights the intricate interplay between O 2*p* hole and the oxygen vacancy in influencing OER efficiency. We therefore suggest that $S_{0.9}Y_{0.1}C$ has an optimal balance between oxygen vacancy and oxygen 2*p* hole is key to achieving superior OER activity. Prior research concluded that a cobalt valence state of +3.3 or +3.4 is optimal for OER activity in cobalt oxides.[20] This is a criterion satisfied by several high-performing catalysts, including $S_{0.9}Y_{0.1}C$. Nevertheless, this valence-state descriptor solely correlates with Co-O covalency (or oxygen 2*p* hole) while neglecting the critical role of oxygen vacancy. Our proposed combination of O 2*p* hole and O vacancy clearly provides a more precise description of OER activity.

To verify the pivotal influence of the interplay between the O 2*p* hole and oxygen vacancy on OER activity, we delved into a detailed discussion of several samples that were featured in Figure 2b. The discussion proceeds in the direction of decreasing O 2*p* hole content. Catalysts like SC-*HP*, SC, and $S_{0.9}Y_{0.1}C$ with adequate oxygen 2*p* hole prefer to catalyze OER through the LOM route, which has a PLS of oxygen vacancy refilling. This is in good agreement with the previous reports.[10,36] SC-*HP* with a nearly maximum oxygen hole but a minute oxygen vacancy suffers from weak hydroxide affinity and poor OER activity. When the oxygen vacancy grows to 0.3, the oxygen 2*p* hole of SC decreases, resulting in improved hydroxide affinity and OER activity. In comparison with the SC catalyst, the $SrCoO_{2.5}$ catalyst exhibits a small drop in OER activity as oxygen vacancy is further increased to 0.5. This is also witnessed by another research.[8] Note that $SrCoO_{2.5}$ has the same level of oxygen 2*p* hole as $LaCoO_3$, on which, theoretically, LOM is thermodynamically unfavorable. However, previous experiments revealed significant and minimum lattice oxygen release on $SrCoO_{2.5}$ and $LaCoO_3$, respectively.[10] This is because the presence of oxygen vacancy favors hydroxide adsorption and in situ oxidation of $SrCoO_{2.5}$ during the OER, resulting in improved Co-O covalency and activated lattice oxygen

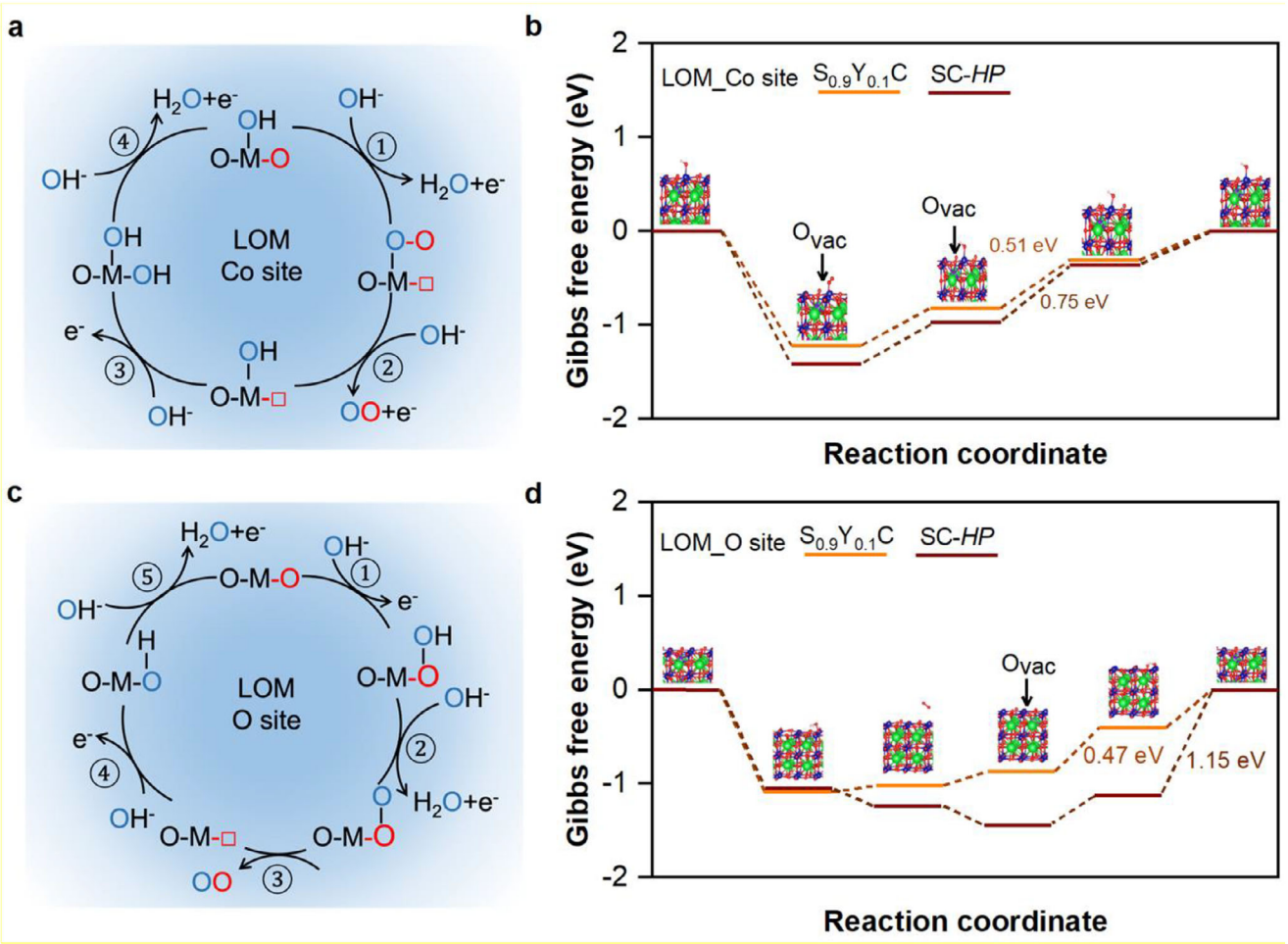

Figure 3. a) Schematic illustration of LOM pathways in alkaline conditions at Co site; and b) corresponding Gibbs free energy diagram at applied potential U = 1.23 V. c) Schematic illustration of LOM pathways in alkaline conditions at O site; and d) corresponding Gibbs free energy diagram at applied potential U = 1.23 V. Gibbs free energy change values for the potential-limiting steps are marked (in eV). The optimized intermediate structures are shown as insets (color code: green for Sr, purple for Y, blue for Co, red for O, and pale pink for H).

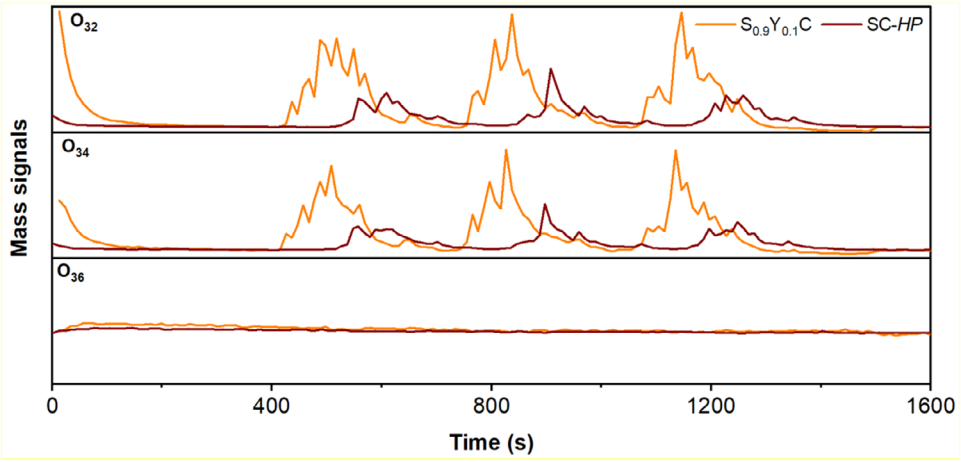

Figure 4. Operando ^{18}O isotope labeling measurement results.

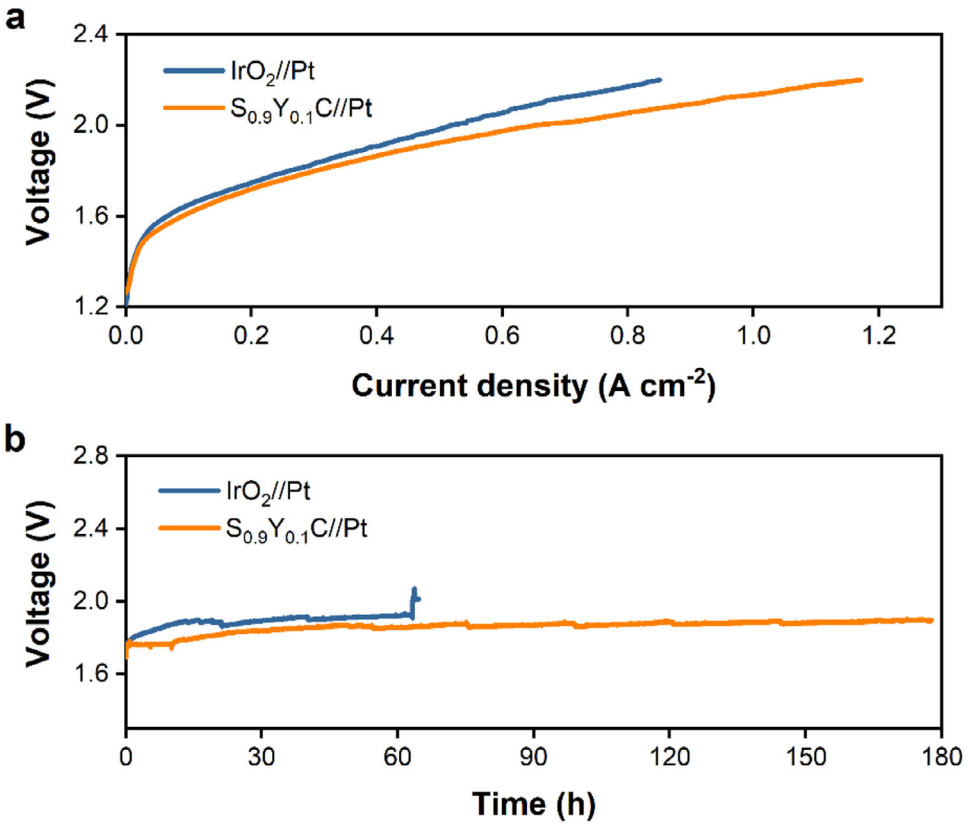

Figure 5. a) Polarization curves and b) Stability test at a current density of 200 mA cm^{-2} of the anion exchange membrane electrolyzers with IrO_2//Pt and $S_{0.9}Y_{0.1}C$//Pt.

(hole-rich oxygen). Nevertheless, the in situ oxidation is confined to the surface regions, leaving the subsurface lattice oxygens of $SrCoO_{2.5}$ to stay in the inactive state. This will undermine the contribution of bulk lattice oxygen to the OER since the diffusion of bulk hole-rich lattice oxygen is also crucial to improved OER activity via the LOM.[37] Therefore, excessive oxygen vacancies do more harm than good to the OER. When the oxygen 2*p* hole falls below 0.5, catalysts prefer to catalyze OER via the conventional AEM, which typically possess larger overpotentials. Catalysts with a small oxygen hole have poor conductivity and low chemical potential.[38] The O-O coupling is no longer a chemical step but instead becomes the PLS, as suggested by DFT Calculations conducted on CoO (in this study) and $LaCoO_3$ in ref.[10] In a word, the optimal catalyst should have a balanced oxygen hole and oxygen vacancy, which prefers the LOM-O route with improved hydroxide affinity. $S_{0.9}Y_{0.1}C$ possesses a trade-off content between oxygen 2*p* hole and oxygen vacancy, located between those of $SrCoO_{2.5}$ and SC samples, thus showing the highest OER activity.

Considering the excellent intrinsic OER activity exhibited by $S_{0.9}Y_{0.1}C$ in the traditional three-electrode system, we further evaluated its water splitting performance by coupling it with Pt cathode (a good hydrogen evolution reaction catalyst) in an anion exchange membrane electrolyzer (Figure S10, Supporting Information) at a temperature of 50 °C. The $S_{0.9}Y_{0.1}C$//Pt catalyst pair achieved a large current density of 700 mA cm^{-2} at 2.01 V at 50 °C (**Figure 5a**), outperforming the state-of-the-art IrO_2//Pt catalyst pair (2.13 V @ 700 mA cm^{-2}). Furthermore, the $S_{0.9}Y_{0.1}C$//Pt electrode stably delivered a current density of 200 mA cm^{-2} for ≈180 h with a potential increment of only 159 mV, much better than that of the IrO_2//Pt catalyst pair (Figure 5b). The water splitting performance exhibited by $S_{0.9}Y_{0.1}C$//Pt catalyst is also better than the well-known BSCF catalyst (coupled with Pt cathode),[39] demonstrating the superiority of balanced oxygen hole and oxygen vacancy in catalyzing the water oxidation.

3. Conclusion

In conclusion, by analyzing a series of cobaltite perovskites, we were able to establish a correlation between OER activity/mechanism and oxygen hole/vacancy. We argue that a pair of competing factors, oxygen 2*p* hole and oxygen vacancy, simultaneously determine the intrinsic OER activity. The increase in oxygen 2*p* hole facilitates direct O-O coupling by activating the lattice oxygen, but reduces hydroxide affinity. The moderate increase in oxygen vacancy lifts the hydroxide affinity, while excessive oxygen vacancy will impede the bulk oxygen involved in the OER. A balance between oxygen 2*p* hole and oxygen vacancy results in a superior LOM-O pathway and appropriate hydroxide affinity on $S_{0.9}Y_{0.1}C$, hence the best OER intrinsic activity. In addition, these findings can be used to explain the OER intrinsic activity of previously reported cobaltite perovskites. More importantly, since the debate regarding the underlying reason for the favorable OER performance has been ongoing for years, we believe that the

viewpoint raised in this study offers a more reasonable descriptor for the design of superior OER electrocatalysts. The long-term persistence of the LOM mechanism under extended OER operation needs further exploration.

Supporting Information

Supporting Information is available from the Wiley Online Library or from the author.

Acknowledgements

G.C. and Y.Y. contributed equally to this work. This work was supported by the Program for Jiangsu Specially-Appointed Professors (R2023T05), the Startup Foundation for Introducing Talent of NUIST (2024R078), the Natural Science Foundation of Jiangsu Province (BK20240707), the Hong Kong Polytechnic University (Project Nos. 1-CE2Z, Q-CDBG, and 1-WZ5L). The authors acknowledge support from Prof. Zhichuan Xu (NTU, Singapore) and the Max Planck-POSTECH-Hsinchu Center for Complex Phase Materials.

Conflict of Interest

The authors declare no conflict of interest.

Data Availability Statement

The data that support the findings of this study are available from the corresponding author upon reasonable request.

Keywords

lattice oxygen, oxygen 2p hole, oxygen evolution, oxygen vacancy, perovskite

Received: October 10, 2025
Revised: November 10, 2025
Published online: November 20, 2025

[1] X. Zhong, L. Sui, M. Yang, T. Koketsu, M. Klingenhof, S. Selve, K. G. Reeves, C. Ge, L. Zhuang, W. H. Kan, M. Avdeev, M. Shu, N. Alonso-Vante, J.-M. Chen, S.-C. Haw, C.-W. Pao, Y.-C. Chang, Y. Huang, Z. Hu, P. Strasser, J. Ma, *Nat. Catal.* **2024**, *7*, 546.
[2] Y. Huang, Z. Wang, H. Xiao, Q. Liu, X. Wang, *J. Am. Chem. Soc.* **2024**, *146*, 29006.
[3] Y. Li, G. Chen, L. Fei, W. Zhou, Z. Shao, *Adv. Funct. Mater.* **2024**, *34*, 2417880.
[4] Y. Li, G. Chen, H.-C. Chen, Y. Zhu, L. Xu, T. Liu, J. Dai, H. Huang, W. Zhou, Z. Shao, *Energy Environ. Sci.* **2023**, *16*, 3331.
[5] X. Cheng, E. Fabbri, Y. Yamashita, I. E. Castelli, B. J. Kim, M. Uchida, R. Haumont, I. P. Orench, T. J. Schmidt, *ACS Catal.* **2018**, *8*, 9567.
[6] W. T. Hong, R. E. Welsch, Y. Shao-Horn, *J. Phys. Chem. C* **2016**, *120*, 78.
[7] J. Suntivich, K. J. May, H. A. Gasteiger, J. B. Goodenough, Y. Shao-Horn, *Science* **2011**, *334*, 1383.
[8] J. T. Mefford, X. Rong, A. M. Abakumov, W. G. Hardin, S. Dai, A. M. Kolpak, K. P. Johnston, K. J. Stevenson, *Nat. Commun.* **2016**, *7*, 11053.
[9] G. Chen, W. Zhou, D. Guan, J. Sunarso, Y. Zhu, X. Hu, W. Zhang, Z. Shao, *Sci. Adv.* **2017**, *3*, 1603206.
[10] A. Grimaud, O. Diaz-Morales, B. Han, W. T. Hong, Y.-L. Lee, L. Giordano, K. A. Stoerzinger, M. T. M. Koper, Y. Shao-Horn, *Nat. Chem.* **2017**, *9*, 457.
[11] W. T. Hong, K. A. Stoerzinger, Y.-L. Lee, L. Giordano, A. Grimaud, A. M. Johnson, J. Hwang, E. J. Crumlin, W. Yang, Y. Shao-Horn, *Energy Environ. Sci.* **2017**, *10*, 2190.
[12] E. Marelli, J. Gazquez, E. Poghosyan, E. Müller, D. J. Gawryluk, E. Pomjakushina, D. Sheptyakov, C. Piamonteze, D. Aegerter, T. J. Schmidt, M. Medarde, E. Fabbri, *Angew. Chem., Int. Ed.* **2021**, *60*, 14609.
[13] Z. Xiao, Y.-C. Huang, C.-L. Dong, C. Xie, Z. Liu, S. Du, W. Chen, D. Yan, L. Tao, Z. Shu, G. Zhang, H. Duan, Y. Wang, Y. Zou, R. Chen, S. Wang, *J. Am. Chem. Soc.* **2020**, *142*, 12087.
[14] L. Zhang, H. Jang, H. Liu, M. G. Kim, D. Yang, S. Liu, X. Liu, J. Cho, *Angew. Chem., Int. Ed.* **2021**, *60*, 18821.
[15] C. Jing, L. Li, Y.-Y. Chin, C.-W. Pao, W.-H. Huang, M. Liu, J. Zhou, T. Yuan, X. Zhou, Y. Wang, C.-T. Chen, D.-W. Li, J.-Q. Wang, Z. Hu, L. Zhang, *ACS Nano* **2024**, *18*, 14496.
[16] H. Sun, X. Xu, Y. Song, W. Zhou, Z. Shao, *Adv. Funct. Mater.* **2021**, *31*, 2009779.
[17] X. Lin, Y.-C. Huang, Z. Hu, L. Li, J. Zhou, Q. Zhao, H. Huang, J. Sun, C.-W. Pao, Y.-C. Chang, H.-J. Lin, C.-T. Chen, C.-L. Dong, J.-Q. Wang, L. Zhang, *J. Am. Chem. Soc.* **2022**, *144*, 416.
[18] Y. Zhou, S. Sun, J. Song, S. Xi, B. Chen, Y. Du, A. C. Fisher, F. Cheng, X. Wang, H. Zhang, Z. J. Xu, *Adv. Mater.* **2018**, *30*, 1802912.
[19] Y. Zhu, G. Chen, Y.-C. Chu, C.-S. Hsu, J. Wang, C.-W. Tung, H. M. Chen, *Angew. Chem., Int. Ed.* **2022**, *61*, 202211142.
[20] J. Zhou, L. Zhang, Y.-C. Huang, C.-L. Dong, H.-J. Lin, C.-T. Chen, L. H. Tjeng, Z. Hu, *Nat. Commun.* **2020**, *41*, 1984.
[21] F. Calle-Vallejo, N. G. Inoglu, H.-Y. Su, J. I. Martınez, I. C. Man, M. T. M. Koper, J. R. Kitchin, J. Rossmeisl, *Chem. Sci.* **2013**, *4*, 1245.
[22] Y. Zhu, L. Zhang, B. Zhao, H. Chen, X. Liu, R. Zhao, X. Wang, J. Liu, Y. Chen, M. Liu, *Adv. Funct. Mater.* **2019**, *29*, 1901783.
[23] W. Zhou, M. Zhao, F. Liang, S. C. Smith, Z. Zhu, *Mater. Horiz.* **2015**, *2*, 495.
[24] S. Balamurugan, E. Takayama-Muromachi, *J. Solid State Chem.* **2006**, *179*, 2231.
[25] Y. Li, Y. N. Kim, J. Cheng, J. A. Alonso, Z. Hu, Y.-Y. Chin, T. Takami, M. T. Fernandez-Díaz, H.-J. Lin, C.-T. Chen, L. H. Tjeng, A. Manthiram, J. B. Goodenough, *Chem. Mater.* **2011**, *23*, 5037.
[26] J. Van Elp, J. L. Wieland, H. Eskes, P. Kuiper, G. A. Sawatzky, F. M. F. De Groot, T. S. Turner, *Phys. Rev. B* **1991**, *44*, 6090.
[27] R. H. Potze, G. A. Sawatzky, M. Abbate, *Phys. Rev. B* **1995**, *51*, 11501.
[28] Y. Zhu, H. A. Tahini, Z. Hu, Z.-G. Chen, W. Zhou, A. C. Komarek, Q. Lin, H.-J. Lin, C.-T. Chen, Y. Zhong, M. T. Fernández-Díaz, S. C. Smith, H. Wang, M. Liu, Z. Shao, *Adv. Mater.* **2020**, *32*, 1905025.
[29] S. I. Csiszar, M. W. Haverkort, Z. Hu, A. Tanaka, H. H. Hsieh, H.-J. Lin, C. T. Chen, T. Hibma, L. H. Tjeng, *Phys. Rev. Lett.* **2005**, *95*, 187205.
[30] M. W. Haverkort, Z. Hu, J. C. Cezar, T. Burnus, H. Hartmann, M. Reuther, C. Zobel, T. Lorenz, A. Tanaka, N. B. Brookes, H. H. Hsieh, H.-J. Lin, C. T. Chen, L. H. Tjeng, *Phys. Rev. Lett.* **2006**, *97*, 176405.
[31] Y. Y. Chin, Z. Hu, H.-J. Lin, S. Agrestini, J. Weinen, C. Martin, S. Hébert, A. Maignan, A. Tanaka, J. C. Cezar, N. B. Brookes, Y.-F. Liao, K.-D. Tsuei, C. T. Chen, D. I. Khomskii, L. H. Tjeng, *Phys. Rev. B* **2019**, *100*, 205139.
[32] A. Grimaud, K. J. May, C. E. Carlton, Y.-L. Lee, M. Risch, W. T. Hong, J. Zhou, Y. Shao-Horn, *Nat. Commun.* **2013**, *4*, 2439.
[33] X. Xu, Y. Pan, Y. Zhong, C. Shi, D. Guan, L. Ge, Z. Hu, Y.-Y. Chin, H.-J. Lin, C.-T. Chen, H. Wang, S. P. Jiang, Z. Shao, *Adv. Sci.* **2022**, *9*, 2200530.
[34] Y. Zhu, W. Zhou, Z.-G. Chen, Y. Chen, C. Su, M. O. Tadé, Z. Shao, *Angew. Chem., Int. Ed.* **2015**, *54*, 3897.

[35] G. Chen, Z. Hu, Y. Zhu, Z.-G. Chen, Y. Zhong, H.-J. Lin, C.-T. Chen, L. H. Tjeng, W. Zhou, Z. Shao, *J. Mater. Chem. A* **2018**, *6*, 9854.
[36] J. S. Yoo, X. Rong, Y. Liu, A. M. Kolpak, *ACS Catal.* **2018**, *8*, 4628.
[37] Y. Pan, X. Xu, Y. Zhong, L. Ge, Y. Chen, J.-P. M. Veder, D. Guan, R. O'Hayre, M. Li, G. Wang, H. Wang, W. Zhou, Z. Shao, **2002**, *Nat. Commun.*, *11*, 2002.
[38] G. Chen, C. Wei, Y. Zhu, H. Huang, *EcoMat* **2022**, *5*, 12294.
[39] E. Fabbri, M. Nachtegaal, T. Binninger, X. Cheng, B.-J. Kim, J. Durst, F. Bozza, T. Graule, R. Schäublin, L. Wiles, M. Pertoso, N. Danilovic, K. E. Ayers, T. J. Schmidt, *Nat. Mater.* **2017**, *16*, 925.